Red photoluminescence and blue-shift caused by phase transformation in multilayer films of titanium dioxide and zinc sulfide

Byeongdae Choi,[1]* Hyunseok Shim[1] and Bunyod Allabergenov[2]

[1] *Division of Nano & Energy Convergence Research, Daegu Gyeongbuk Institute of Science and Technology (DGIST), 50-1 Sang-Ri, Hyeonpung-Myeon, Dalseong-Gun, Daegu 711-873, South Korea*
[2]*Department of Information & Nano Materials Engineering School of Advanced Materials & System Engineering Kumoh National Institute of Technology, Daehak-ro 61, Gyungbuk,Gumi 730-701, South Korea*
[*]*bdchoi1@dgist.ac.kr*

Abstract: The most versatile methods for altering the properties and behavior of materials involve a phase transformation in the solid state. In this article, we report multilayered films of $ZnS/TiO_2/ZnS$ on amorphous SiO_x/Si substrates by pulsed laser deposition (PLD). After sequential vacuum annealing at various temperatures, we investigated the effects of TiO_2 on the phase transformation of ZnS films and the consequential changes in photoluminescence (PL) property. PL spectra of the film revealed red emission centered at 686 nm after annealing at 600 °C, however, this emission disappears, and the color shifts to blue after annealing at 700 °C. Detailed analysis identified that TiO_2 acts as a catalytic agent for the phase transformation of ZnS at this temperature, and that the color shift to blue resulted from decreased red emissions attributed to oxygen in the film. The present results show that catalytic agent-mediated phase transformation has strong potential for the modification of material properties.

OCIS codes: (310.0310) Thin films; (310.6860) Thin films, optical properties; (250.0250) Optoelectronics; (250.5230) Photoluminescence.

References and links

1. A. G. Guy, "Reconstructive and displacive phase transformations," Metall. Mater. Trans., B, Process Metall. Mater. Proc. Sci. **3**, 2535–2536 (1972).
2. V. Raghavan and M. Cohen, "Solid-state phase transformations," Treatise on Solid State Chemistry **5**, 67–127 (1975).
3. S. H. Tolbert and A. P. Alivisatos, "Size dependence of a first order solid-solid phase transition: the wurtzite to rock salt transformation in CdSe nanocrystals," Science **265**(5170), 373–376 (1994).
4. F. Liu, F. Sommer, C. Bos, and E. J. Mittemeijer, "Analysis of solid state phase transformation kinetics: models and recipes," Int. Mater. Rev. **52**(4), 193–212 (2007).
5. Y. Peng, F. Wang, Z. Wang, A. M. Alsayed, Z. Zhang, A. G. Yodh, and Y. Han, "Two-step nucleation mechanism in solid-solid phase transitions," Nat. Mater. **14**(1), 101–108 (2014).
6. J. Tao, T. Luttrell, and M. Batzill, "A two-dimensional phase of TiO_2 with a reduced bandgap," Nat. Chem. **3**(4), 296–300 (2011).
7. K. Mahmood, M. Asghar, N. Amin, and A. Ali, "Phase transformation from cubic ZnS to hexagonal ZnO by thermal annealing," J. Semicond. **36**(3), 033001 (2015).
8. R. S. McWilliams, D. K. Spaulding, J. H. Eggert, P. M. Celliers, D. G. Hicks, R. F. Smith, G. W. Collins, and R. Jeanloz, "Phase transformations and metallization of magnesium oxide at high pressure and temperature," Science **338**(6112), 1330–1333 (2012).
9. S. Deka and P. A. Joy, "Enhancement of the phase transformation temperature of γ-Fe_2O_3 by Zn^{2+} doping," J. Mater. Chem. **17**(5), 453–456 (2007).
10. V. I. Ivashchenko, P. E. A. Turchi, and V. I. Shevchenko, "Phase transformation B1 to B2 in TiC, TiN, ZrC and ZrN under pressure," Condens. Matter Phys. **16**(3), 33602 (2013).
11. L. W. Shacklette and W. S. Williams, "Influence of order-disorder transformations on the electrical resistivity of vanadium carbide," Phys. Rev. B **7**(12), 5041–5046 (1993).

#244225 Received 2 Jul 2015; revised 26 Aug 2015; accepted 3 Sep 2015; published 8 Sep 2015

12. C. Maier, O. Blaschko, and W. Pichl, "Influence of uniaxial deformation on the phase transformation in lithium," Phys. Rev. B Condens. Matter **52**(13), 9283–9290 (1995).
13. M. Golosovsky, Y. Neve-Oz, D. Davidov, and A. Frenkel, "Phase shift on reflection from metallodielectric photonic bandgap materials," Phys. Rev. B **70**(11), 115105 (2004).
14. H. Zhang, F. Huang, B. Gilbert, and J. F. Banfield, "Dynamics simulations, thermodynamic analysis, and experimental study of phase stability of zinc sulfide nanoparticles," J. Phys. Chem. B **107**(47), 13051–13060 (2003).
15. C. A. Feigl, A. S. Barnard, and S. P. Russo, "Size- and shape-dependent phase transformations in wurtzite ZnS nanostructures," Phys. Chem. Chem. Phys. **14**(28), 9871–9879 (2012).
16. Z. Li, B. Liu, S. Yu, J. Wang, Q. Li, B. Zou, T. Cui, Z. Liu, Z. Chen, and J. Liu, "The study of structural transition of ZnS nanorods under high pressure," J. Phys. Chem. C **115**(2), 357–361 (2011).
17. S. B. Qadri, E. F. Skelton, A. D. Dinsmore, J. Z. Hu, W. J. Kim, C. Nelson, and B. R. Ratna, "The effect of particle size on the structural transitions in zinc sulfide," J. Appl. Phys. **89**(1), 115–119 (2001).
18. S. Desgreniers, L. Beaulieu, and I. Lepage, "Pressure-induced structural changes in ZnS," Phys. Rev. B **61**(13), 8726–8733 (2000).
19. Z. Wang, L. L. Daemen, Y. Zhao, C. S. Zha, R. T. Downs, X. Wang, Z. L. Wang, and R. J. Hemley, "Morphology-tuned wurtzite-type ZnS nanobelts," Nat. Mater. **4**(12), 922–927 (2005).
20. H. E. Swanson and R. K. S. Fuyat, "X-ray diffraction powder patterns," Natl. Bur. Stand. Circ. **539**, 14–19 (1953).
21. S. D. Mo and W. Y. Ching, "Electronic and optical properties of three phases of titanium dioxide: Rutile, anatase, and brookite," Phys. Rev. B Condens. Matter **51**(19), 13023–13032 (1995).
22. S. Hamad, C. R. A. Catlow, S. M. Woodley, S. Lago, and J. A. Mejías, "Structure and stability of small TiO_2 nanoparticles," J. Phys. Chem. B **109**(33), 15741–15748 (2005).
23. J. Muscat, V. Swamy, and N. M. Harrison, "N. M. First-principles calculations of the phase stability of TiO_2," Phys. Rev. B **65**(22), 224112 (2002).
24. H. Feng, M. H. Zhang, and L. E. Yu, "Phosphorus-doped TiO_2 catalysts with stable anatase-brookite biphase structure: synthesis and photocatalytic performance," J. Nanosci. Nanotechnol. **13**(7), 4981–4989 (2013).
25. H. M. Lu, W. X. Zhang, and Q. Jiang, "Phase stability of nanoanatase," Adv. Eng. Mater. **5**(11), 787–788 (2003).
26. D. A. H. Hanaor and C. C. Sorrell, "Review of the anatase to rutile phase transformation," J. Mater. Sci. **46**(4), 855–874 (2011).
27. H. T. Evans Jr, and E. D. McKnight, "New wurtzite polytypes from Joplin, Missouri," Am. Mineral. **44**, 1210–1218 (1959).
28. J. S. King, E. Graugnard, and C. J. Summers, "Photoluminescence modification by high-order photonic bands in TiO_2/ZnS:Mn multilayer inverse opals," Appl. Phys. Lett. **88**(8), 081109 (2006).
29. B. Allabergenov, S. H. Chung, S. M. Jeong, S. Kim, and B. Choi, "Enhanced blue photoluminescence realized by copper diffusion doping of ZnO thin films," Opt. Mater. Express **3**(10), 1733–1741 (2013).
30. J. D. Reyes, R. S. Ojeda, C. R. S. Espíndola, M. G. Arellano, and O. Z. Moran, "Structural and optical characterization of wurtzite type ZnS," Curr. Appl. Phys. **15**(2), 103–109 (2015).

1. Introduction

Materials that have more than two stable phases undergo phase transformations with changes in the ambient conditions such as temperature and pressure [1–10]. For device applications, this phase transformation is an important reaction that affects device performance because the characteristics of materials such as strength, conductivity, and bandgap are generally altered by the phase transformation [11–13]. For example, wide bandgap semiconductor ZnS generally has two stable phases: sphalerite [cubic ($F4_3m$)] and wurtzite [hexagonal ($P6_3mc$)]. The sphalerite phase is more stable than the wurtzite phase at low temperatures under the pressure of 1 bar. At 1020 °C, ZnS undergoes a massive transformation to the wurtzite phase under the pressure of 1 bar. Thus, the bandgap of ZnS increases from 3.54 to 3.8 eV [14]. In addition, structural defects generated during the phase transformation can create deep-level energy bands that modify the opto-electrical properties of the material. So far, many investigations for the phase transformation of ZnS at lower temperature than normal condition have been reported. A recent study has shown that the temperature for this ZnS phase transformation decreases with the particle size, and nanometer-sized sphalerite particles transform to the wurtzite phase at an annealing temperature of 400 °C [15]. The pressure as well as the particle size has been shown to reduce the phase transition temperature. In fact, the sphalerite-to-wurtzite phase transformation has been observed at a high pressure of 30 GPa at room temperature [16–18]. Recently, morphology-tuned high-pressure phase transformations have been found in nanomaterials. Wurtzite ZnS nanobelts exhibited the wurtzite-to-

#244225 Received 2 Jul 2015; revised 26 Aug 2015; accepted 3 Sep 2015; published 8 Sep 2015

sphalerite phase transformation with the fracture of the nanobelts [19]. However, few investigations on the phase transformation of ZnS caused by the lattice mismatch have been reported. At the atomic-scale, the lattice mismatch between stacked materials with different lattice constants can affect the phase transformation because the lattice mismatch imposes extensive pressure on the interfacial atoms. In this article, by stacking and annealing TiO_2 and ZnS, they have similar lattice constants, we investigated the phase transformation of ZnS, and the consequential changes in photoluminescence. The multilayered films were prepared through sequential pulsed laser deposition (PLD) of ZnS and TiO_2 and were annealed at high temperatures. To suppress unwanted strain effects on the phase transformation caused by crystalline substrates, we used amorphous substrates. The results show that the recrystallization of the rutile (TiO_2) phase induces a displacive phase transformation of ZnS to reduce the lattice mismatch. Photoluminescence (PL) spectra reveal that the amorphous phase formation during the phase transformation provides ZnS with oxygen ions, which results in red emission.

2. Experimental

Thin films were prepared with pulsed laser deposition (PLD) using a KrF excimer laser (wavelength: 248 nm). To suppress unwanted strain effects on the phase transformation caused by crystalline substrates, we used amorphous substrates. The thermally oxidized silicon substrates were ultrasonically sequentially cleaned with acetone and alcohol for 15 min before drying in air. After transferring the substrate to a holder block through the load-lock chamber, the PLD chamber was pumped to 2×10^{-7} Torr prior to deposition. To promote stoichiometric reactions of ZnS, Ar gas was flowed in a rate of 30 sccm, and the working pressure was held at 200 mTorr during the deposition. To investigate the film phases caused by the deposition temperature, we prepared ZnS thin films with a thickness of 200 nm on substrates at room temperature (RT) and at 500 °C. The multilayer films were formed on the substrates through the sequenced deposition of ZnS and TiO_2 at room temperature (RT) and at 500 °C. The KrF excimer laser was irradiated on target surfaces 5 cm above the substrate for 10 and 3 min at a repetition rate of 2 Hz to deposit the 100 nm thick ZnS film and the 20 nm thick TiO_2 film, respectively. Cylindrical pellets (4×20 mm^2) of ZnS (Sigma-Aldrich, 99.99%) and TiO_2 (Sigma-Aldrich, 99.99%) for the PLD targets were prepared by spark plasma sintering at 750 °C under 30 MPa pressure. To promote crystallization of the films after deposition, the films were annealed for 30 min at 500, 600, and 700 °C using a tube furnace, while Ar gas flowed at a rate of 30 sccm to maintain the 200 mTorr pressure and to prevent oxidation of ZnS during annealing. The PL properties were evaluated at RT (excitation wavelength: 300 nm) with a photospectrometer (JASCO FP-6500, Light source: Xe lamp). Crystallography and cross-sectional structures of the films were measured with an X-ray diffractometer (Bruker, D2 PHASER, CuKα, $\lambda = 0.15406$ nm) and high resolution-scanning transmission electron microscopy (HR-STEM; JSM-6701F).

3. Results and discussion

3.1 Phase transformation in sphalerite-ZnS/TiO_2/sphalerite-ZnS thin films

In order to investigate the phase transformation of ZnS, we need to prepare the sphalerite phase. First, we prepared ZnS thin films with a thickness of 200 nm on substrates at room temperature (RT) and 500 °C to examine the film phases caused by the deposition temperature.

#244225 Received 2 Jul 2015; revised 26 Aug 2015; accepted 3 Sep 2015; published 8 Sep 2015

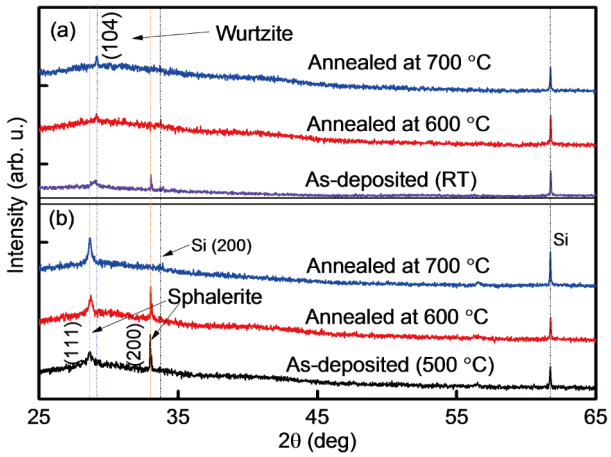

Fig. 1. The XRD patterns of ZnS thin films on SiO_x/Si substrates prepared by pulsed laser deposition and annealed at various temperatures for 30 min. (a) deposited at RT, (b) 500 °C.

The ZnS film deposited at RT in Fig. 1(a) reveals two peaks of (104) and (200) caused by the wurtzite and sphalerite phases of ZnS, respectively. After annealing the samples at 600 °C, the (200) peak decreases, and the (104) peak becomes dominant. When the film was deposited at 500 °C, the X-ray diffraction (XRD) patterns showed two peaks at similar angles as those of films prepared at RT. Comparing Figs. 1(a) and 1(b), the peak at smaller angle slightly shifted from (104), corresponding to the peak from the (111) plane of the sphalerite phase [20]. Paradoxically, the wurtzite phase, which is stable at high temperature, condenses on substrate at room temperature, while the sphalerite phase condenses at 500 °C. However, this paradox is not impossible because PLD is not an equilibrium process, and the surface mobility of the RT depositions is not high enough to reconstruct the deposits for a more stable phase of the sphalerite.

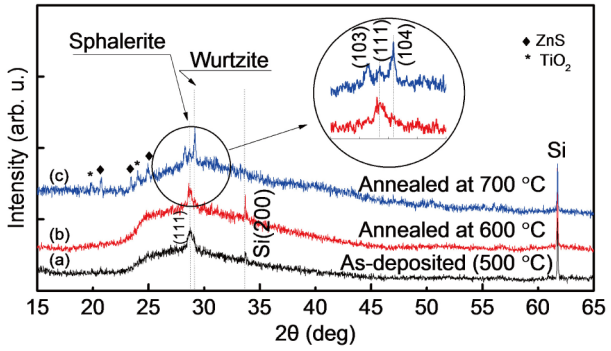

Fig. 2. The XRD patterns of the multilayer ZnS/TiO_2/ZnS films on SiO_x/Si substrates prepared at 500 °C by pulsed laser deposition and annealed at various temperatures for 30 min. (a) as-deposited, (b) 600 °C, (c) 700 °C.

On the other hand, in this experiment, a sandwiched structure with a TiO_2 middle layer is favorable for protecting TiO_2 from unwanted reactions with ambient impurities during annealing. To satisfy these conditions, we prepared multilayer films of ZnS/TiO_2/ZnS with thicknesses of 100/20/100 nm through sequential deposition of ZnS, TiO_2, and ZnS in a 200 mTorr Ar atmosphere at 500 °C, because ZnS predominately crystallizes the sphalerite phase at 500 °C, as shown in Fig. 1. Figure 2 shows the XRD patterns of the multilayered films annealed at various temperatures. The as-deposited film of Fig. 2(a) reveals the same peaks of

#244225 Received 2 Jul 2015; revised 26 Aug 2015; accepted 3 Sep 2015; published 8 Sep 2015

(111) as those shown in the ZnS film prepared at 500 °C [See Fig. 1(b)]. After annealing the film at 600 °C [Fig. 2(b)], no remarkable changes in the XRD patterns were observed. However, the sample annealed at 700 °C shows two additional peaks [Fig. 2(c)]. Besides the (111) peak of the sphalerite phase, the (103) and (104) peaks of the wurtzite phase were developed, as shown in the inset of the Fig. 2 [20]. At this temperature, no phase transformation has been observed in single structure films [See Fig. 1(b)]. However, this evolution is feasible through the TiO_2-mediated phase transformation of ZnS.

For detailed analysis, we performed TEM investigations of the films.

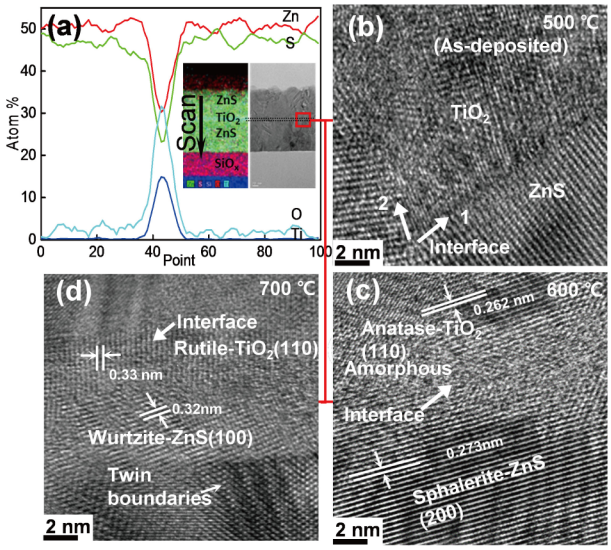

Fig. 3. The STEM analysis of the multilayer ZnS/TiO_2/ZnS films on SiO_x/Si substrates prepared at 500 °C and annealed at various temperatures. (a) the atom mass-% profile, the insets represent the cross-sectional image and the mapping image for elements, (b) the HR-TEM images for the as-deposited film, (c) after annealing at 600 °C, (d) after annealing at 700 °C.

Figure 3(a) shows atom mass-% profile for the elements of the film, and the insets show the energy dispersed spectroscopy (EDS) mapping for the elements and the cross-section of the film, respectively, which indicate that TiO_2 was deposited between the ZnS layers as anticipated. The TEM images of Figs. 3(b)–3(d) present the detailed interfacial structures of TiO_2 and ZnS in the films deposited at 500 °C without annealing and in the films annealed at 600 and 700 °C, respectively. In the as-deposited film, the anatase phase of TiO_2 makes a sharp interface [Fig. 3(b), arrow 1] with the sphalerite phase. In some areas of the film [Fig. 3(b), arrow 2], the phases are mixed at the interface, which may depend on the crystalline orientation of the materials. However, after annealing at 600 °C, we could observe the amorphous phase at the interface [See Fig. 3(c)]. Further increasing the annealing temperature to 700 °C, we observed that the amorphous phase decreases and the rutile phase of TiO_2 crystallizes [See Fig. 3(d)]. The anatase-to-rutile phase transformation of TiO_2 is reconstructive; the amorphous phase generally appears during the phase transformation [21–25]. Since we annealed the sample at 200 mTorr vacuum, the formation of the amorphous phase at this low temperature was unexpected because the transformation temperature inversely depends on the working pressure [26].

One possible reason for the evolution of the amorphous phase is the lattice mismatch between the anatase phase and the sphalerite phase. The mismatch between the most prevailing orientations of the ZnS (111) plane and anatase (001) plane is calculated to be over 51%. The anatase phase deposited on the ZnS (111) plane is severely strained by the lattice

#244225 Received 2 Jul 2015; revised 26 Aug 2015; accepted 3 Sep 2015; published 8 Sep 2015

mismatch, which could activate the phase transformation at a lower temperature than normal. Figure 3(d) shows that the rutile phase crystallizes from the amorphous phase at 700 °C. The amorphous phase was significantly decreased compared to that shown in Fig. 3(c). Surprisingly, the sphalerite phase transformed to the wurtzite phase at the interface with the rutile TiO_2 (110) phase. Moreover, the twin boundaries appearing in the figure strongly support the occurrence of the massive ZnS phase transformation. Because our samples were annealed in a 200 mTorr vacuum, without the help of catalytic agents, the sphalerite phase cannot transform to the wurtzite phase at this temperature. In particular, no phase transformation occurs in the sphalerite phase at 700 °C when there are no additives such as TiO_2 [See Fig. 1(b)], which provides evidence that TiO_2 acted as a catalytic agent for the phase transformation of ZnS in this structure. The driving force for this phase transformation is the lattice mismatch of the sphalerite phase with the growing rutile phase. The rutile (110) plane (d_{110} = 0.323 nm) has a 0.3% lattice misfit with the wurtzite (104) plane (d_{104} = 0.324 nm), but a 3.5% mismatch with the sphalerite (111) plane (d_{111} = 0.312 nm). Therefore, the transformation to the wurtzite phase is favorable for releasing the strain caused by the lattice mismatch.

3.2 Photoluminescence in red range for sphalerite-ZnS/TiO_2/sphalerite-ZnS thin films

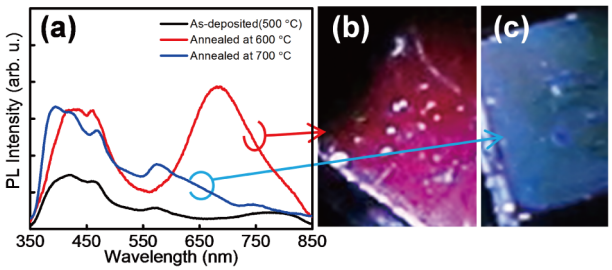

Fig. 4. The PL properties of the multilayer ZnS/TiO_2/ZnS films on SiO_x/Si substrates prepared at 500 °C and annealed at various temperatures (a) the PL spectra, (b) the emission image of the films obtained by digital camera after annealing at 600 °C, (c) 700 °C.

The more interesting results of this experiment are that PL property of the film changes during the phase transformation. Figure 4(a) shows PL spectra of the films after annealing at various temperatures. The as-deposited film emits luminescence at 420, 465, and 572 nm. These emissions were caused by interstitial sulfur, zinc vacancy, and sulfur vacancy, respectively [27, 28]. Subsequently, red emission dramatically appears at 686 nm (1.81 eV) in the sample annealed at 600 °C; however, this emission disappears, and the color shifts to blue after annealing at 700 °C, as shown in Figs. 4(b) and 4(c), respectively. Metal-ion-doped ZnS does not have a red emission, but oxygen traps have been reported as deep acceptor levels that allow red emission [29, 30]. The red emission could probably be attributed to an oxygen trap, and the amorphous phase of TiO_2 serves as a source for the oxygen ion. From Fig. 3(c), TiO_2 forms an amorphous phase at the interface with ZnS at 600 °C, allowing oxygen ions to easily diffuse into ZnS. When the annealing temperature is increased to 700 °C, the oxygen ions trapped in ZnS are diffused and crystallize the rutile phase, and the deep acceptor levels for red emission are diminished as a result.

3.3 Characterization of wurtzite-ZnS/TiO_2/wurtzite-ZnS thin films

To verify this concept, we made another combination of the wurtzite and the anatase structure by depositing films at RT. In Fig. 5(a), the XRD patterns of the films show that no ZnS phase transformation occurs due to high temperature annealing. After annealing the samples at 500 °C, like the single layer films shown in Fig. 1(a), the (200) peak decreases, and the (104) and the (006) peak of wurtzite become dominant. In addition, the primary (104) peak of wurtzite

#244225 Received 2 Jul 2015; revised 26 Aug 2015; accepted 3 Sep 2015; published 8 Sep 2015

is prevailed after annealing at 700 °C. Figure 5(b) shows the cross-section of the film. Figures 5(c) and 5(d) show the EDS mapping and atom mass-% profile for the elements of the film, respectively. The TEM images in Figs. 5(e) and 5(f) present the detailed interfacial structures of TiO_2 and ZnS in the film deposited at RT after annealing at 500 and 600 °C, respectively.

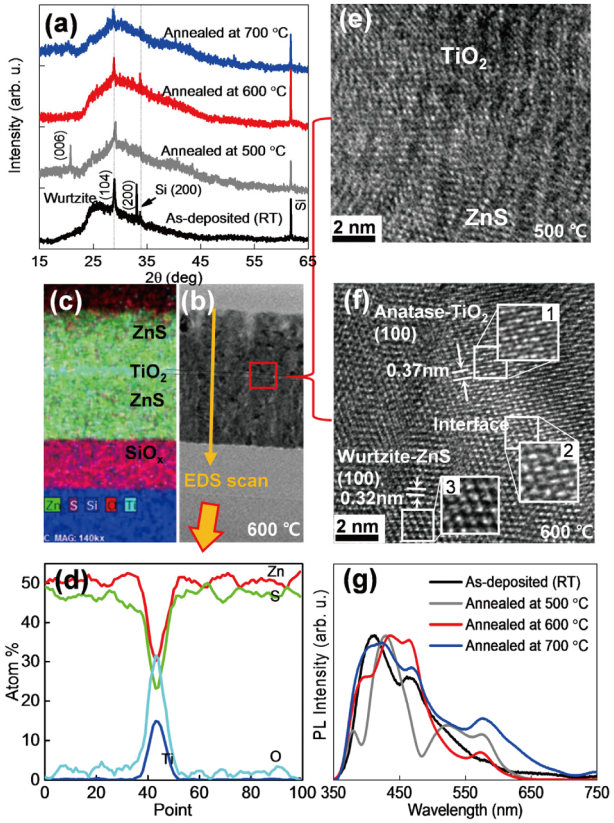

Fig. 5. Characteristics of the multilayer ZnS/TiO_2/ZnS films on SiO_x/Si substrates prepared at RT. (a) the XRD patterns of the films according to the annealing temperature, (b) the cross-sectional TEM image of the film after annealing at 600 °C, (c) the mapping image for elements, (d) the atom mass-% profile, (e) the HR-TEM image for the film after annealing at 500 °C, (f) after annealing at 600 °C. Inset images 1, 2, and 3 are the magnifications of the areas for the anatase phase, interfaces and the wurtzite phase, respectively, (g) the normalized PL spectra for the films after annealing at various temperatures.

In Fig. 5(e), the interfaces are not clear, but this could be due to the poor crystallinity of the films. After annealing at 600 °C we could observe clear images for each phase [Fig. 5(f)]. The insets 1, 2, and 3 represent the unit cells of the anatase, mixed interface, and wurtzite structure, respectively. The anatase structure does not melt at 600 °C in this combination, but the structure mixes with the wurtzite structure at the interface. The 13.5% lattice mismatch with interplanar spacings of 0.37 and 0.32 nm for the anatase and wurtzite phases, respectively, is insufficient to promote the phase transformation of TiO_2 at the interface. The PL spectra of Fig. 5(g) represent the common emission centers for the ZnS samples. In this combination, we could not observe the red emission caused by the oxygen traps in the induced phase transformation of TiO_2 in the samples annealed at high temperatures.

4. Conclusion

In summary, we observed the phase transformation of ZnS from the sphalerite to the wurtzite phase by the catalytic activity of TiO_2 deposited on the ZnS sphalerite phase. The anatase

#244225 Received 2 Jul 2015; revised 26 Aug 2015; accepted 3 Sep 2015; published 8 Sep 2015

phase of TiO_2 has a large lattice mismatch with the sphalerite and transformed to the amorphous phase after annealing at 600 °C. On the other hand, the rutile phase reconstructively crystallized during annealing at 700 °C. Moreover, to reduce the lattice mismatch with the rutile phase, a massive phase transformation from the sphalerite-to-wurtzite phase of ZnS was observed at temperatures much lower than 1020 °C under normal conditions. The optical properties of multilayered film were drastically changed by the phase transformation. In particular, red emission, which was caused by an oxygen trap, was observed in the sample annealed at 600 °C.

Acknowledgments

This work was supported by the basic research program (15-NB-05) through the Daegu Gyeongbuk Institute of Science and Technology (DGIST), funded by the Ministry of Science, ICT, and future planning of Korea.

#244225 Received 2 Jul 2015; revised 26 Aug 2015; accepted 3 Sep 2015; published 8 Sep 2015